Structure Analysis in Polyurethane Foams at Interfaces

Nasir Mahmood, Jörg Kressler, Karsten Busse

Fachbereich Ingenieurwissenschaften, Martin-Luther-Universität Halle-Wittenberg, D-06099 Halle (Saale), Germany

Received 8 September 2004; accepted 1 February 2005
DOI 10.1002/app.22243
Published online in Wiley InterScience (www.interscience.wiley.com).

ABSTRACT: The aim of this study was to investigate the structure and morphology of polyurethane (PU) foams at the interface with a thermoplastic material. Fourier transform infrared/attenuated total reflectance spectroscopy was used to study the reaction of 4,4′-diphenylmethane diisocyanate (MDI) with polyether-based polyols with water as a blowing agent via the absorption intensity of the ν(NCO, 2265 cm^{-1}) vibrational band of MDI in three different PU foam systems. The data revealed that MDI reacted simultaneously with two different species in the reaction mixture having different reaction rates. These were the reactions of isocyanate functional groups with water (fast reaction) and polyol (slow reaction). A structure analysis at the PU foam interface (i.e., PU formed a compact film 110 ± 30 μm thick at the interface) with a thermoplastic material plate was carried out with small-angle X-ray scattering (SAXS), transmission electron microscopy (TEM), and neutron reflection (NR) techniques. From SAXS measurements, a typical hard-segment–segment distance of 10 ± 0.3 nm was observed. The TEM and NR data of the compact PU film revealed an internal layered structure (parallel to the surface) with a typical layer thickness of 260–400 nm. The formation of a layered morphology (macrophase-separated structures) was assumed to be due to the difference in the polarities of the hard and soft segments. Furthermore, the layer thickness increased when D_2O was used as the blowing agent instead of H_2O. © 2005 Wiley Periodicals, Inc. J Appl Polym Sci 98: 1280–1289, 2005

Key words: interfaces; neutron reflectivity; polyurethanes; SAXS; TEM

INTRODUCTION

Polyurethane (PU) foams are cellular or expanded materials synthesized by the reaction of diisocyanate with polyol in the presence of a blowing agent. According to the mechanical properties, PU foams are categorized as flexible, rigid, or semirigid materials. PU foams are multiblock copolymers considered to consist of alternating hard and soft segments.[1] The soft segments are composed of long-chain polyethers or polyesters, which exhibit flexibility [low glass-transition temperature (T_g) part] and elastomeric properties at room temperature. The reaction of hydroxyl groups with isocyanate groups forms linkages based on urethane structures (high T_g part). Additionally, water present in a typical PU foam formulation will react with isocyanate to produce CO_2 and urea-based hard segments. The heat evolved from the exothermic reactions along with the CO_2 generation helps to blow the foaming mixture and gives the foam its cellular character. The long hard-segment structures segregate together because of similarities in polarity and hydrogen bonding to form a pseudocrosslinked network structure.[2] These segregated structures provide substantial stability to the foam material.[3]

Because of the complex nature of the PU foam structure and morphology development, the use of model systems has been very important for the study of the different aspects of PU foams, especially at interfaces. The reactivity and concentration of the reactants in PU foam formulations have a strong influence on the development of PU foam morphology. Many authors have employed Fourier transform infrared (FTIR) spectroscopy to investigate both the reaction kinetics and the morphology development during the foaming process.[4–6] The phase separation of polyurea segments can be monitored through hydrogen-bonding studies during the PU foam reaction process.[7] By using FTIR spectroscopy, Rossmy et al.[8,9] showed that in the initial stages of the reaction process, the formed urea hard segments stay in solution, but at a certain level of the reaction, they separate as a second phase because of their concentration and molecular weight development. The adhesion of a PU foam on a thermoplastic (TP) material depends significantly on the interfacial structures of both materials. Kim et al.[10] showed by X-ray scattering on an interface between a rigid PU foam and zinc phosphated steel some crystallite structures, and they found that these crystallites contribute to the interface strength. The same authors also claimed that the number of these crystalline structures is much more important than their size.[11] Other authors believe that the hard segments contribute

Correspondence to: K. Busse (karsten.busse@iw.uni-halle.de).

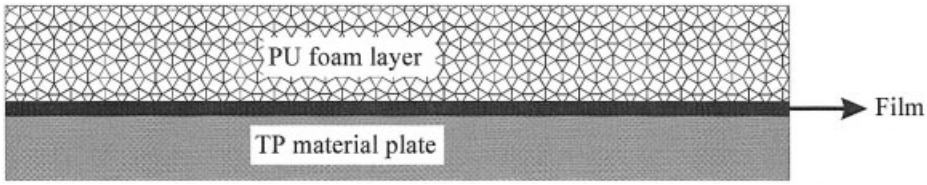

Figure 1 Schematic representation of a PU foam layer on a TP material surface.

to the hydrogen bonding/chemical bonding at an interface according to the nature of the substrate material.[12,13]

In this article, we present the results for the structure analysis of the interface between three different PU foam systems and a TP material plate. The TP material plate was a blend composed of polycarbonate, acrylonitrile butadiene styrene, and styrene maleic anhydride. The PU foams were prepared directly on a horizontally fixed TP material plate with 4,4′-diphenylmethane diisocyanate (MDI), polyether-based polyols, and water and deuterium oxide as blowing agents. The reaction in the PU foam systems was monitored with the Fourier transform infrared/attenuated total reflectance (FTIR–ATR) technique via the absorption intensity of the ν(NCO) vibrational band due to asymmetric stretching vibrations of the isocyanate group at 2265 cm^{-1}. Small-angle X-ray scattering (SAXS), neutron reflection (NR), and transmission electron microscopy (TEM) techniques were employed for the structure analysis. At the interface between the PU foam and TP, a compact PU film, 110 $\pm$ 30 μm thick, was formed (see Fig. 1). Investigating the inner structure of this PU film, we found a layered morphology parallel to the surface with a typical thickness of 260–400 nm for each layer. It is assumed that a phase separation between hydrophilic poly(ethylene oxide) (PEO) and hydrophobic polypropylene (PPO) blocks of the polyol in an early stage of reaction is the origin of this structure.

EXPERIMENTAL

Materials

All the chemicals for the PU foam and the TP material plates were used as obtained. MDI with an isocyanate index of 88 (the isocyanate index is the molar ratio of isocyanate groups to active hydrogen-bearing groups, i.e., hydroxyl and amino groups) was used. The polyether polyols were PPO- and PEO-based with a weight ratio of 80 : 20 PPO/PEO. Different catalysts and crosslinkers were added to the mixtures.[14–16] Three different PU formulation were used (PU-a, PU-b, and PU-c), and their details are reported in Table I. To differentiate between the usage of H_2O and D_2O as blowing agents, either an "h" or a "d" was added to the name (e.g., d-PU-a for a deuterated PU foam of formulation "a"). When a climate treatment was also performed, this was indicated by an additional "-T" in the name (e.g., h-PU-a-T).

Preparation of the PU foam samples

To prepare the samples with PU foam adhering to TP material plate, an appropriate amount of polyol was mixed with MDI and mechanically stirred for some seconds. Finally, the reacting mixture was transferred to a foaming tool, which already contained the TP material plate. The tool was then closed to allow the process to proceed for 10 min at 40°C. After that time, the foamed plate was removed from the foaming tool. The foam samples with deuterium oxide were prepared with D_2O as an indirect blowing agent instead of H_2O.

To reduce the adhesion of the PU foam samples on the TP material plate, a climate treatment was performed by the placement of some samples in a climate chamber (model Excal 2221 HA, Climats/Sapratin, St. Médard d'Eyrans, France). The details about the climate cycle are explained in Figure 2. The foam samples were separated from the interface, and then the compact PU film was removed from the bulk foam surface. A thickness of 110 $\pm$ 30 μm for this PU film was measured with a micrometer screw.

FTIR spectroscopy

FTIR measurements were carried out on a PerkinElmer S2000 FTIR spectrometer (Wellesley, MA) equipped with a Golden Gate diamond single attenuated total reflectance (ATR) cell heatable up to 200°C from LOT Oriel (Darmstadt, Germany). A small portion of the PU foam reaction mixture was placed on a preheated (40°C) ATR cell, and spectra were recorded with 50-s intervals. The change in the intensity of the isocyanate band was used

TABLE I
Formulation Details of PU Foam Systems

Foaming system	Polyol (g)	Isocyanate (g)	H_2O/D_2O (g)
PU-a	100	45	2.6
PU-b	100	44	2.8
PU-c	100	54	3.1

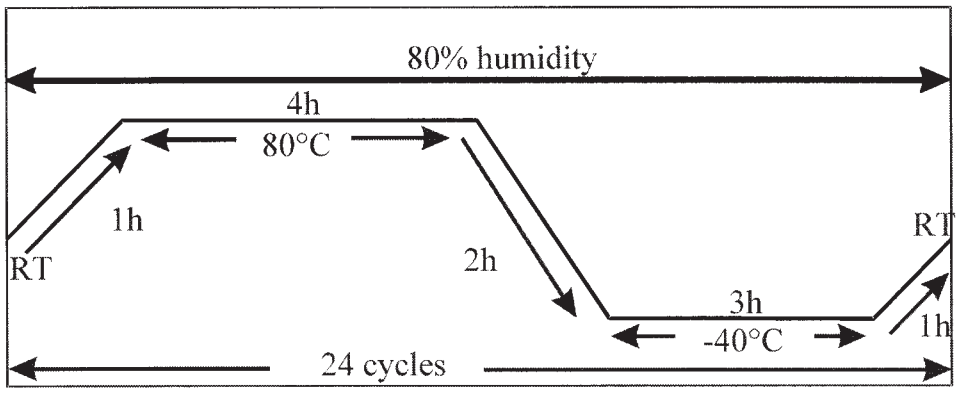

Figure 2 Schematic representation of a single climate cycle. Each cycle takes 11 h and is carried out 24 times (RT = room temperature).

to calculate the reaction time for each reacting foam mixture.

SAXS

The compact PU film was powdered after cooling in liquid nitrogen. The powdered samples were filled in glass capillaries for measurements. SAXS intensities were detected with a Siemens Hi-Star two-dimensional area detector (Siemens, Berlin, Germany) and integrated. Cu Kα radiation with a wavelength of $\lambda = 0.154$ nm was used. The scattering vector ($\mathbf{q}$) is defined by $\mathbf{q} = (4\pi/\lambda)\sin\theta$.

TEM

The TEM images were obtained on a LEO 912 transmission electron microscope (LEO/Zeiss, Oberkochen, Germany) with an accelerating voltage of 120 kV. The compact PU film from the interface was microtomed perpendicularly to the surface after cooling in liquid nitrogen. TEM micrographs were acquired from thin samples after staining in RuO_4, which is sensitive for hard segments.[25]

NR

The foam samples were separated from the interface, as schematically shown in Figure 3, and the flat PU foam surface was exposed to the NR instrument (HADAS) at the Jülich Research Centre (Germany). These experiments were carried out with a two-dimensional position-sensitive detector and neutrons with a wavelength of 4.52 Å.

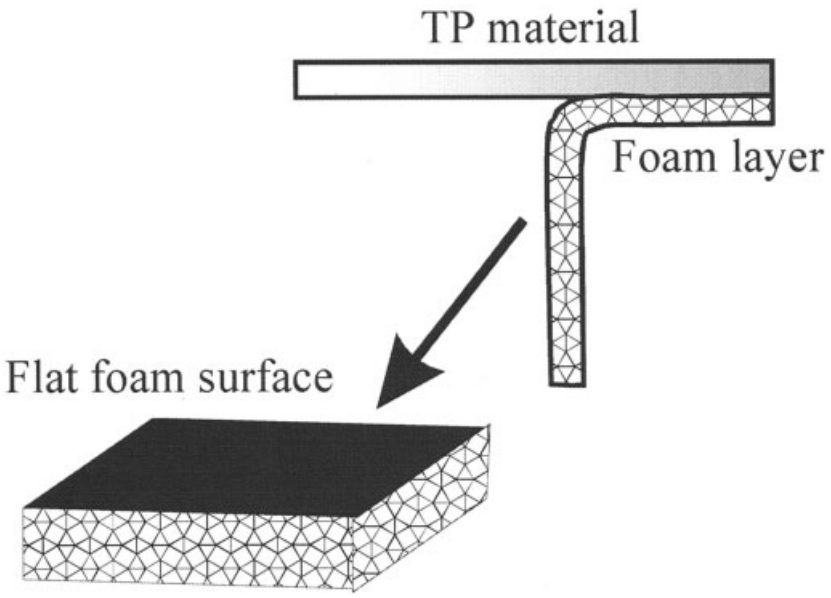

Figure 3 Schematic representation of the separation of a PU foam/TP material interface: a flexible PU foam layer is removed from a TP material in a way similar to a peel test. The flat PU foam surface is exposed to NR reflection studies.

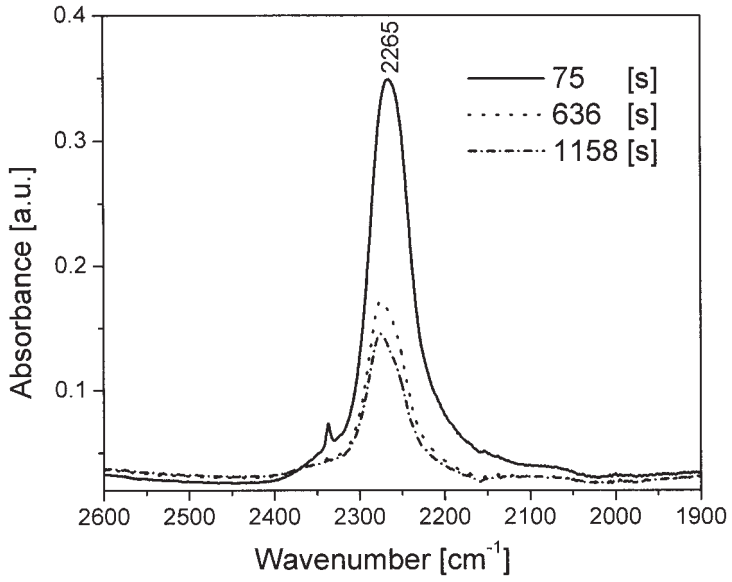

Figure 4 FTIR–ATR spectra of the isocyanate absorption band (2265 cm^{-1}) during the reaction process with polyol and water in the h-PU-a foam system at 40°C at different times after the mixing of the components.

RESULTS AND DISCUSSION

FTIR spectroscopy

Representative infrared (IR) spectra for the reaction process of the isocyanate part of MDI with polyether polyols and water are shown in Figure 4. This region is useful for studying the reaction process, as the band at 2265 cm^{-1} includes the isocyanate asymmetric stretching vibrations. The decrease in the intensity of this band was used to monitor the conversion of isocyanate functional groups as a function of the reaction process with polyol and water in three different PU foam systems.

The first measurement after the reaction mixture was placed on an ATR cell shows for the integrated area of the 2265-cm^{-1} peak the highest value, which decreases continuously with time. Representative results for the h-PU-a foam system at 40°C are shown in Figure 5. The curve depicted in Figure 5 can be fitted by biexponential decay functions [eq. (1)], and the obtained parameters are given in Table II:

$$y = y_0 + A_1 e^{-t/t_1} + A_2 e^{-t/t_2} \quad (1)$$

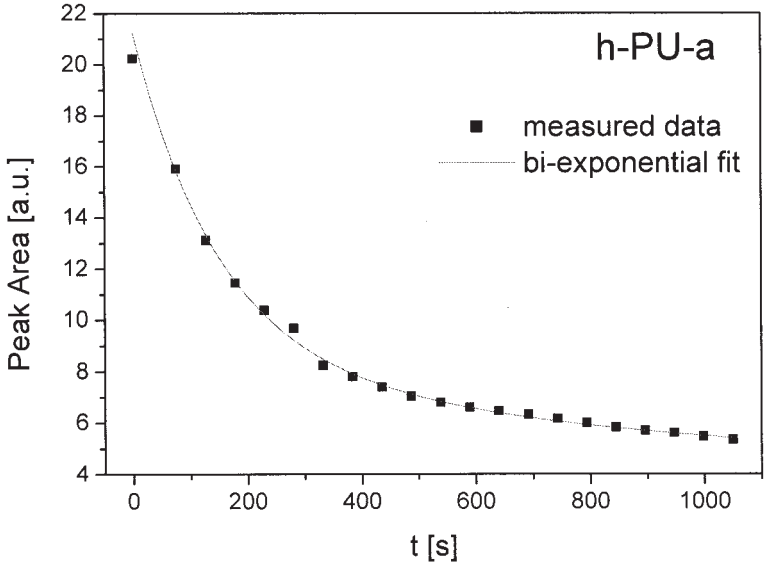

Figure 5 Integrated peak area of the isocyanate absorption band (2265 cm^{-1}) as a function of time. The data are fitted to a biexponential decay function.

TABLE II
Reaction Times (s) Obtained by the Fitting of a Bi-Exponential Decay Function to the Peak Area of the Isocyanate Absorption Band (2265 cm^{-1})

Reaction time	Foam system		
	h-PU-a	h-PU-b	h-PU-c
t_1	146 ± 10	73 ± 7	72 ± 7
t_2	850 ± 100	600 ± 70	350 ± 40

In this equation, y is the measured peak area at time t, with constant background y_0, amplitudes A_1 and A_2, and decay times t_1 and t_2. The assumption of a biexponential decay is the simplest one for these kinds of reactions, excluding initialization and termination.[17]

The observed timescales indicate that the isocyanate in the reaction mixture is following two different reaction kinetics, that is, reacting with two different species. Accordingly, t_1 and t_2 represent fast and slow reactions of the isocyanate, respectively. Rossmy et al.[8] reported that water is more reactive in PU foam formulations than polyether polyol and aromatic amines. Therefore, t_1 should correspond to the reaction of isocyanate with water, and t_2 should correspond to the reaction of isocyanate with polyols.

The three foam formulations differ not only in the water content but also in the additives. These additives strongly influence the isocyanate conversion. The three foam formulations can be described as slow, intermediate, and fast foams. These observed differences in the three foam systems are ordered as expected according to the chosen additives. Finally, formulation PU-c shows the fastest reaction with water and polyol, whereas PU-a shows the slowest.

Figure 6 demonstrates the influence of the formulation differences and reaction rate on the structure/morphology development. Observing the time dependence of the absorption bands between 1730 and 1630 cm^{-1}, we can follow the formation of urethane, hy-

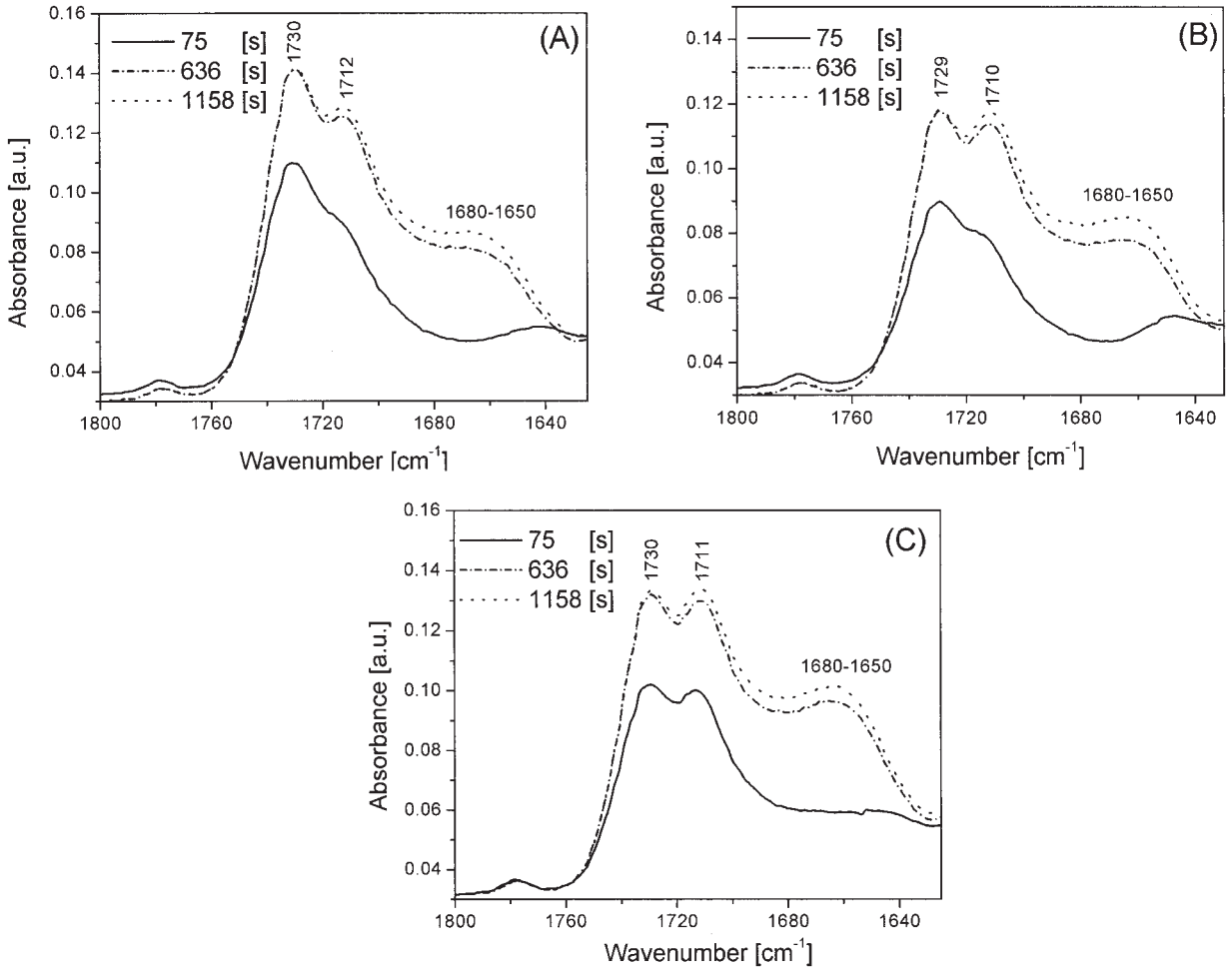

Figure 6 FTIR–ATR spectra in the carbonyl region at different times during the reaction process of isocyanate with polyol and water in three different PU foam systems at 40°C: (A) h-PU-a, (B) h-PU-b, and (C) h-PU-c. The absorbance bands associated with urethane (1730 cm^{-1}), soluble urea and hydrogen-bonded urethane (1700–1715 cm^{-1}), and hydrogen-bonded urea (1650–1680 cm^{-1}) groups are labeled on the respective absorption bands.

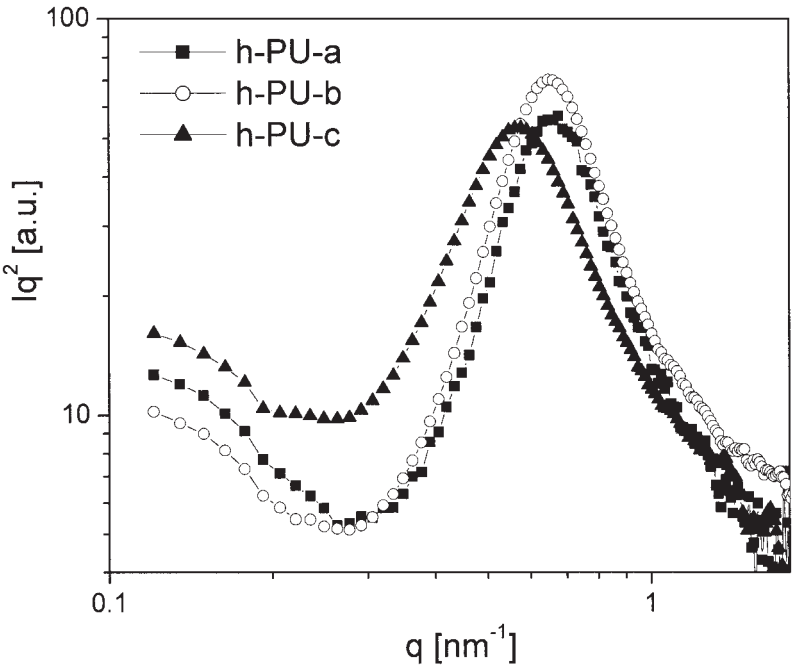

Figure 7 Lorentz- and background-corrected SAXS traces for powders of compact PU film in three different foam systems with water as an indirect blowing agent. The peaks correspond to the average hard-segment distance in the sample.

drogen-bonded urethane and urea, and nonbonded urea. According to Elwell et al.,[18] the formation of non-hydrogen-bonded urethane (1730 cm^{-1}) and nonbonded urea (1715 cm^{-1}) evolves early in the reaction. The formation of these two structures takes place simultaneously, not sequentially, as early research had suggested.[8,19,20] Both signals (1730 and 1715 cm^{-1}) can be seen clearly in the figure, but the slowest foam with less water [h-PU-a; Fig. 6(A)] has a weak urea signal at 1715 cm^{-1}. Foam h-PU-b [Fig. 6(B)], with a faster urea-forming process, has an increased urea signal, whereas foam h-PU-c [Fig. 6(C)], with the highest amount of water, also has the most intense urea signal. It is also apparent from the figure that there is an induction time before the formation of hydrogen-bonded urea; that is, microphase separation of urea hard segments occurs in all the investigated foam systems (indicated by the 1650–1680-cm^{-1} band). The intensity of the broad band linked with hydrogen-bonded urea (1650–1680 cm^{-1}) in each foam system is also related to the extent of phase separation.

SAXS

The SAXS measurements were carried out to study the hard-segment distances[21–24] in compact PU films at the interface. These studies were performed on deuterated and nondeuterated samples, respectively. The determined SAXS profiles for compact PU films of nondeuterated samples are shown in Figure 7. The intensity (I) values have been rescaled and Lorentz-corrected ($I\mathbf{q}^2$), and a Porod background ($I \sim \mathbf{q}^{-4}$) has been subtracted. The bulk samples were also measured (the results are not given here), and the peak was at the same position found for the compact film samples.

A significant peak was observed in each measurement, and it corresponds to a typical hard-segment distance in the sample. The hard-domain distance was calculated with Bragg's law: $d = 2\pi/q_{max}$. q_{max} is the position of the peak, estimated by the subtraction of a monotonic background (Porod) and then fitting with a Gaussian. The hard-domain distances do not differ in h-PU-a and h-PU-b, but differences exist between h-PU-c and the other two samples (Table III). In the low $\mathbf{q}$ range, the curves differ from each other, and that is due to the inner surface effect.

The SAXS profiles for partially deuterated samples are shown in Figure 8, and the results for these samples are given in Table IV. For the d-PU-a and d-PU-b samples, the peak is nearly at the same position. However, in the d-PU-c sample, the peak position is shifted to low $\mathbf{q}$ values.

TABLE III
Results of SAXS Measurements with H_2O as an Indirect Blowing Agent

Parameter	h-PU-a	h-PU-b	h-PU-c
$\mathbf{q}$ (nm^{-1})	0.65 ± 0.02	0.65 ± 0.02	0.58 ± 0.02
d (nm)	9.7 ± 0.3	9.7 ± 0.3	10.8 ± 0.3

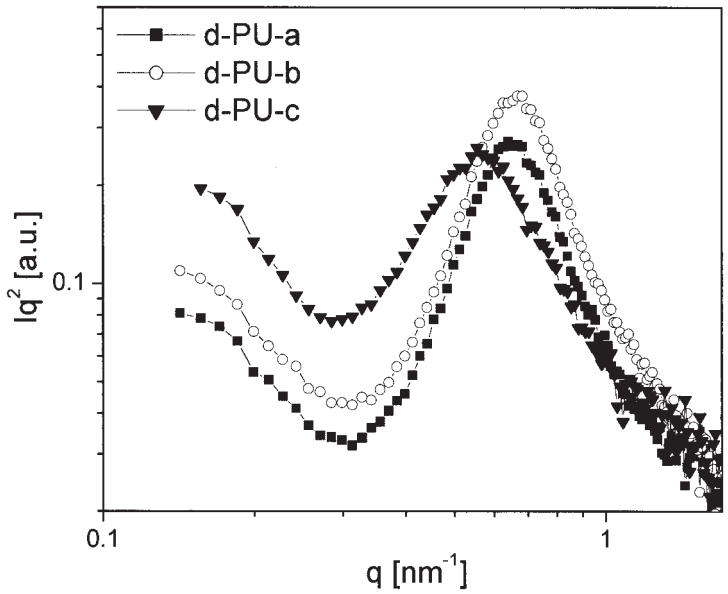

Figure 8 Lorentz- and background-corrected SAXS traces for powders of compact PU film in three different foam systems with D_2O as an indirect blowing agent. The peaks correspond to the average hard-segment distance in the sample.

These SAXS measurements show that the hard-segment distances remain nearly unchanged at the interface with the change of the blowing agent from H_2O to D_2O. These hard segments are embedded in a typical microphase-segregated structure, and according to Armisted et al.,[25] their size does not change with the water content in PU foam formulations. Therefore, it seems that there are also secondary parameters such as crosslinkers that also contribute to the formation of these structures. The used additives also have a strong influence on the formation of urea hard segments. Li et al.[26] studied the effects of chain extenders (additives) on morphology development in flexible PU foams, and they found that with additives the onset of microphase separation was delayed and the interdomain spacing was increased. Our results indicate similar behavior. Hence, the observed difference in the hard-segment distance in the h-PU-c film sample in comparison with the other two systems (h-PU-a and h-PU-b) is due to the formulation difference. A faster reaction with polyol leads to an increased hard-segment distance.

TEM

The TEM images acquired from compact PU film formed at the interface are displayed in Figures 9 and 10 for deuterated and nondeuterated samples, respectively. Elongated structures (arranged in layered form) parallel to the surface in the range of ~400 nm can be seen in the image of the deuterated sample (Fig. 9).

Similar but slightly thinner structures can be observed in a nondeuterated sample of a typical thickness in the range of 260 nm (Fig. 10). The formation of these layered structures at the interface in compact PU

TABLE IV
Results of SAXS Measurements with D_2O as an Indirect Blowing Agent

Parameter	d-PU-a	d-PU-b	d-PU-c
q (nm^{-1})	0.65 ± 0.02	0.66 ± 0.02	0.57 ± 0.02
d (nm)	9.7 ± 0.3	9.5 ± 0.3	11.0 ± 0.4

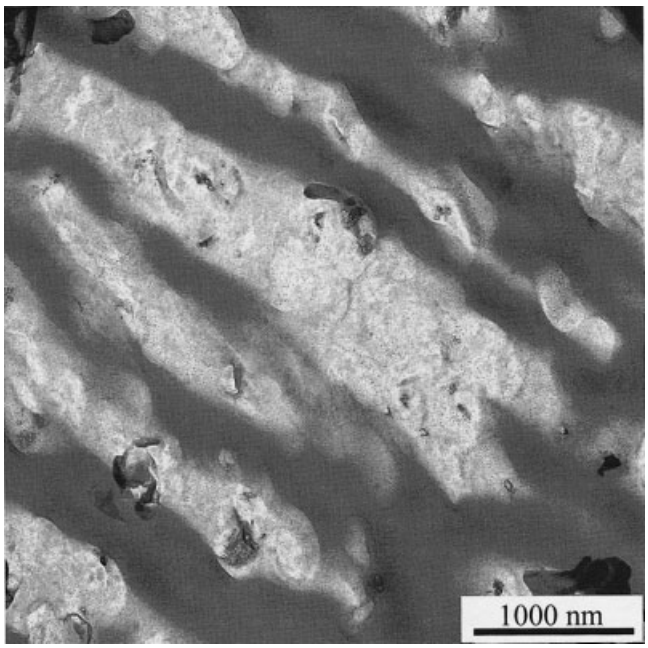

Figure 9 TEM image of a compact PU film sample (d-PU-a) after staining with RuO_4. The elongated structures are parallel to the film surface. A typical layer thickness is 400 nm.

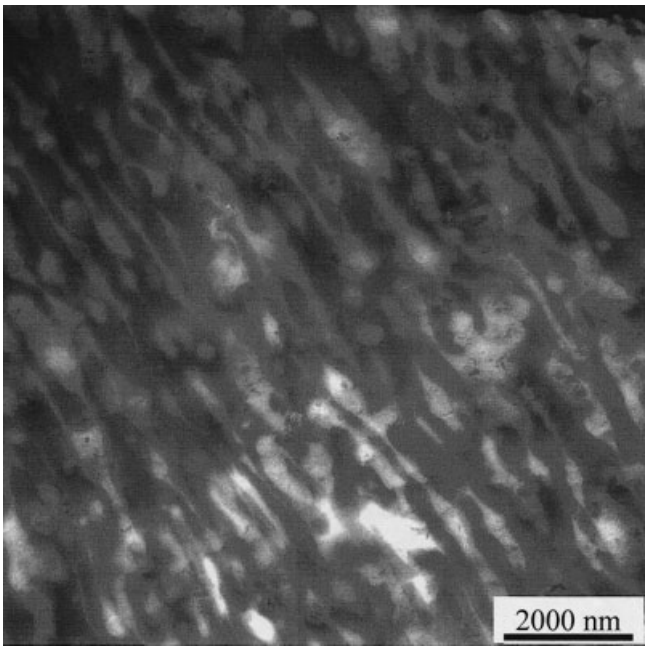

Figure 10 TEM image of a compact PU film sample (h-PU-a) after staining in RuO_4. The elongated structures are parallel to the film surface. A typical layer thickness is 260 nm.

film takes place during the polymerization process through the mechanism of liquid–liquid phase separation. Because of the difference in the hydrophobicity of PPO and PEO, phase separation between a PEO-based polyol and an H_2O-rich phase and a PPO-based polyol and an H_2O-poor phase will start. The more hydrophobic phase with the PPO-based polyol will preferentially cover the surface of the hydrophobic TP material at the interface. As a result of the concentration gradient, the process of phase separation will form a second layer consisting of a PEO-based polyol and an H_2O-rich phase. Finally, an arrangement of layers with different compositions, leading to alternating regions with higher and lower hard-segment densities (elongated structures parallel to the surface in TEM images), is formed at the interface.

The differences in the sizes of elongated structures in deuterated and nondeuterated samples could be due to the reaction process. Rossmy et al.[8,9] showed, using IR spectroscopy of polyethers with different reactivities, that the urea hard segments initially formed stay in solution, but at a certain point they separate as a second phase because of their concentration and molar mass buildup. Therefore, the reactivity will be higher and the time will be less to separate the mixture into equilibrium phases.

The typical hard-segment distance in the range of 10–20 nm, as detected by the previously discussed SAXS measurements, could not be observed in these TEM images. The same effect was described by Neff et al.[27] Their TEM studies in bulk PU foams showed diffuse urea aggregates with a size between 50 and 200 nm, but the internal hard-segment distances were only visible after degradation of the soft segments.

NR

After determining the specular and nonspecular reflection regimes from the measured data, we evaluated **q** with eq. (2), and the representative NR profile for one of the investigated samples (h-PU-a-T) is depicted in Figure 11:

$$q = 4\pi/\lambda^*\sin\,[(\alpha_i+\alpha_f)/2] \qquad (2)$$

where α_i and α_f are the initial and final angles between the sample surface and flight direction of neutrons, respectively, and λ is the neutron wavelength.

In the **q** range of 0.014–0.04 A^{-1}, fluctuations (Kiessig fringes) in the reflection signal can be observed (indicated by vertical lines in Fig. 11). These fluctuations can be fitted by a layered structure of parts with higher (ρ_1) and lower (ρ_2) scattering length densities. From TEM results, we know that two phases with nearly the same thickness and a regular elongated structural arrangement perpendicular to the surface exist in compact PU film. Using the parratt32 program from Christian Braun, HMI,[28] for fitting the results, we obtained the thicknesses for both phases. The differences between the fit and the data above **q** = 0.03 A^{-1} are due to the underlying background from the hard-segment Braggs reflection. In the case of H_2O samples, all layers are in the range of 300 nm. If the thickness of both layers is not in the same range (i.e., the thickness

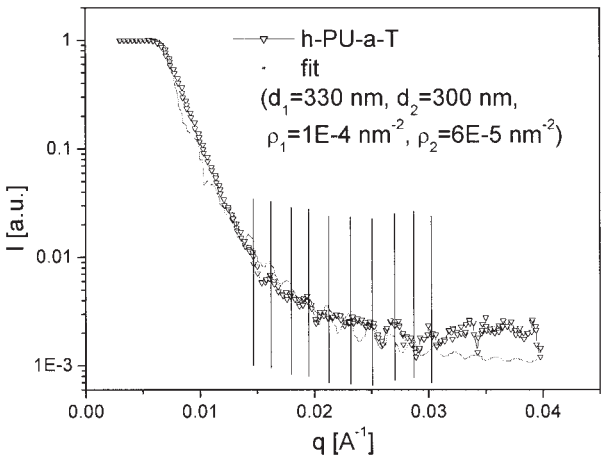

Figure 11 Neutron reflectivity as function of **q** for a PU foam sample (h-PU-a-T). The differences between the fit and the data above **q** = 0.03 A^{-1} is due to the underlying background from the hard-segment Braggs reflection. The vertical lines indicate the significant fluctuations of the measurement.

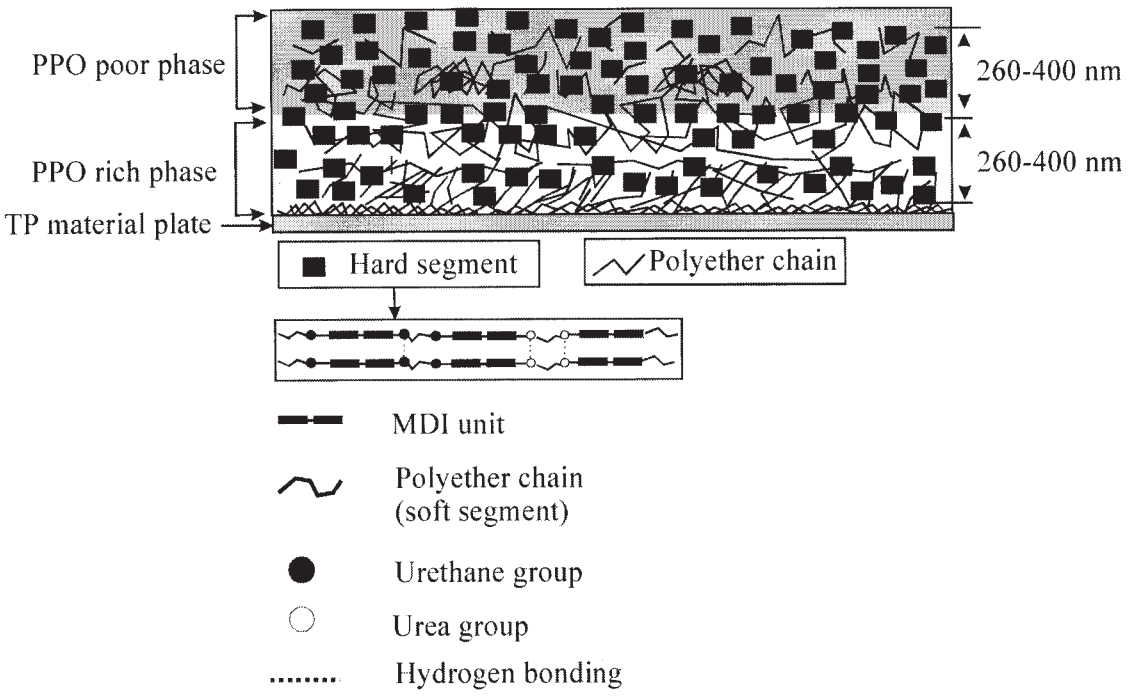

Figure 12 Schematic representation of hard segments and a layered arrangement of aggregate structures in a compact PU film formed at the interface with a TP material plate. The hard-segment distance (10 nm) is detected by SAXS, and the layered arrangement of aggregate structures (260–400 nm) is observed by TEM and NR measurements.

or the volume fraction differs more than 10%), the significance of the fluctuations decrease, and this is observed in the h-PU-c-T sample with $d_1 = 270$ nm and $d_2 = 360$ nm. In the **q** range above 0.04 A^{-1}, which is not depicted in Figure 11, the scattering of the hard segments can be observed. The observed hard-segment distances coincide with the SAXS measurements discussed previously.

Only one of the deuterated samples (d-PU-b-T) shows significant fluctuations, which were fitted with a 400-nm-thick layer system, which is at the limit of the resolution of the instrument. There are several possible reasons that the other samples will show no proper fluctuations: (1) they have thicker layers, as observed in TEM images, and are therefore above the resolution of the instrument; (2) the volume fraction of each phase is not near 50%; and (3) the layer thickness is not homogeneous in the sample.

The NR measurements have shown that the compact PU film at the interface is internally ordered in layered structures. On this basis, we can assign two phases with different (scattering length) densities. These phases do not correspond to hard and soft segments, as the typical hard-segment distances are ~10 nm and the phases have a thickness of ~300 nm. As we observed different scattering length densities, which cannot be assigned to hard and soft segments, and there is no other possibility that the material is macrophase-separated,[29] it can be concluded that the formation of two regions of different scattering length densities is due to the aggregation (formed through a phase-separation mechanism) of hard-segment domains.

For more detail, the difference in the hard-segment distances and the aggregated structures is explained schematically in Figure 12. The hydrophobic TP surface should be covered by a layer of hydrophobic components of the PU foam mixture, that is, with a larger amount of PPO and less water. Depending on the reaction time, the layer thickness may vary, but because of the phase separation of hydrophilic and hydrophobic parts, a second PEO- and water-rich layer will be formed in the next step. Depending on the volume fraction and mobility of the phases, this layered structure can be repeated several times. These layers were observed in TEM and NR measurements. Within each phase, the formation of urea hard segments takes place, preferentially in the PEO- and water-rich phase, as the water is a reaction partner of MDI to finally form urea. In the next step, a microphase separation between hard and soft segments occurs. The hard segments unite through hydrogen bonding and form big aggregates[30] with a typical distance of 10 nm between them, as detected by SAXS.

CONCLUSIONS

From the reaction process of isocyanate, the observed reaction times t_1 and t_2 correspond to the reactions of

water and polyol with isocyanate groups (NCO), respectively. The observed dependence of t_1 and t_2 is in good order according to the formulation differences among three different foam systems. The h-PU-c system shows the fastest reaction with water and polyol, whereas h-PU-a is the slowest formulation. The influence of formulation differences on the morphology development (i.e., the formation of urethane and hydrogen-bonded urethane and urea) was observed by the interpretation of IR spectra in the carbonyl region. The formation of nonbonded urea (1715 cm^{-1}) was lowest in the less reactive foam system in comparison with the other two.

A thin compact PU film at the interface (PU foam/TP material interface), 110 ± 30 μm thick, was found. From the SAXS investigations, the hard-segment distances were observed in PU film samples at the interface. The same segment–segment distance, that is, on the order of $d = 9.7 \pm 0.3$ nm, was observed in h(d)-PU-a and h(d)-PU-b for deuterated and nondeuterated PU film samples. However, in h(d)-PU-c, it was 11.0 ± 0.4 nm and 10.8 ± 0.3 nm for deuterated and nondeuterated PU film samples, respectively. These differences in the hard-segment distances in the three foam systems are due to the different reaction rates. The reaction rate has an influence on the microphase-separation process of hard segments.

TEM and NR measurements showed that the PU film at the interface is internally ordered in a layered morphology. The thickness of the layers ranges from 260 nm for H_2O samples up to 400 nm for D_2O samples. It is concluded that the origin of these layers is phase separation in an early stage of the reaction process (i.e., macrophase separation of hydrophilic and hydrophobic parts). On this basis, we can assign two phases with different (scattering length) densities, and these phases mainly correspond to the macrosegregated structures, as is clear from TEM images.

The authors gratefully acknowledge R. Thomann for the transmission electron microscopy measurements. U. Rücker and A. Wutzler are thanked for their help with the neutron reflection and Fourier transform infrared measurements, respectively.

References

1. Cooper, S.; Tobolsky, A. J Appl Polym Sci 1966, 10, 1837.
2. Dennis, G. L.; Paul, C. In Hand Book of Adhesive Technology; Pizzi, A.; Mittal, K. L., Eds.; Marcel Dekker: New York, 1994; Chapter 24.
3. Moreland, J. C.; Wilkes, G. L.; Turner, R. B.; Rightor, E. G. J Appl Polym Sci 1994, 52, 1459.
4. Elwell, M. J.; Ryan, A. J.; Grunbauer, H. J. M.; VanLieshout, H. C. Polymer 1996, 37, 1353.
5. McClusky, J. V.; Priester, R. D.; O'Neill, R. E.; Willkomm, W. R.; Heaney, M. D.; Capel, M. A. J Cell Plast 1994, 30, 338.
6. Priester, R. D.; McClusky, J. V.; O'Neill, R. E.; Turner, R. B.; Harthcock, M. A.; Davis, B. L. J Cell Plast 1990, 26, 346.
7. Brunette, C. M.; Hsu, S. L.; MacKnight, W. J. Macromolecules 1982, 15, 71.
8. Rossmy, G. R.; Kollmeier, H. J.; Lidy, W.; Schator, H.; Wiemann, M. J Cell Plast 1977, 13, 26.
9. Rossmy, G. R.; Kollmeier, H. J.; Lidy, W.; Schator, H.; Wiemann, M. J Cell Plast 1981, 17, 319.
10. Kim, J.; Ryba, E.; Miller, J. W.; Bai, J. J Adhes Sci Technol 2003, 17, 1351.
11. Kim, J.; Ryba, E. J Adhes Sci Technol 2001, 15, 1747.
12. Sugama, T.; Kukacka, L. E.; Carciello, N.; Warren, J. B. J Mater Sci 1988, 23, 101.
13. Kalpana, S. K.; Marek, W. U. J Coat Technol 2000, 72, 35.
14. Colvin, B. G. Cell Polym 1992, 11, 29.
15. Lowe, D. W.; Arai, S. J Cell Plast 1987, 23, 33.
16. Kaushiva, B. D.; Wilkes, G. L. Polymer 2000, 41, 6981.
17. Hiemenz, P. C. Polymer Chemistry; Marcel Dekker: New York, 1984.
18. Elwell, M. J.; Mortimer, S.; Ryan, A. Macromolecules 1994, 27, 5428.
19. Bailey, F. E.; Critchfield, F. E. J Cell Plast 1981, 17, 333.
20. Merten, R.; Lauerer, D.; Dahm, M. J Cell Plast 1968, 4, 262.
21. Raymond, N.; Adeyinka, A.; Christopher, W. M.; Anthony, J. R. J Polym Sci Part B: Polym Phys 1998, 36, 573.
22. Dimitrios, V. D.; Garth, L. W. J Appl Polym Sci 1997, 66, 2395.
23. Benjamin, C.; Benjamin, S. H. Chem Rev 2001, 101, 1727.
24. James, P. A.; Garth, L. W. J Appl Polym Sci 1998, 35, 601.
25. Armisted, J. P.; Wilkes, G. L.; Turner, R. B. J Appl Polym Sci 1988, 35, 601.
26. Li, W.; Ryan, A. J.; Meier, I. K. Macromolecules 2002, 35, 6306.
27. Neff, R.; Adedeji, A.; Macosko, C. W.; Ryan, A. J. J Polym Sci Part B: Polym Phys 1998, 36, 573.
28. Parratt32 or The Reflectivity Tool. http://www.hmi.de/bensc/instrumentation/instrumente/v6/refl/parratt_en.htm (accessed Aug 2003).
29. Rightor, E. G.; Urquhart, G. S.; Hitchcock, A. P.; Ade, H.; Smith, A. P.; Mitchell, G. E.; Priester, R. D.; Aneja, A.; Appel, G.; Wilkes, G.; Lidy, W. E. Macromolecules 2002, 35, 5873.
30. Shinichi, S.; Yoshihiro, O.; Harunori, S.; Takeshi, N.; Lameck, B.; Shunji, N. J Polym Sci Part B: Polym Phys 2000, 38, 1716.